

Nanocomposites from in-Situ Polymerization of Substituted Polyacetylene within Lamellar Surface of the Montmorillonite: A Solid-State NMR Study

Sangrama K. Sahoo,[†] Dong Wook Kim,[†] Jayant Kumar,[†] Alexandre Blumstein,[‡] and Ashok L. Cholli^{*,†}

Center for Advanced Materials and Department of Chemistry, University of Massachusetts Lowell, Lowell, Massachusetts 01854

Received November 8, 2002; Revised Manuscript Received February 13, 2003

ABSTRACT: Nanocomposites prepared by in-situ polymerization of 2-ethynylpyridine (2EPy) in the presence of a layered aluminosilicate such as Ca^{2+} -montmorillonite (MMT) were characterized by solid-state ^{13}C cross-polarization/magic angle spinning (CP/MAS) NMR spectroscopy. The structure and dynamics of the polymer layer inserted between the montmorillonite lamellae were investigated. The ^{13}C NMR chemical shifts of the polymer component of the nanocomposite that was prepared by in-situ polymerization were assigned by analyzing the difference between the chemical shift values of the bulk and bulk-intercalated poly(2-ethynylpyridine) (P2EPy) nanocomposite material. The results of solid-state NMR and X-ray diffraction studies clearly demonstrate a spontaneous polymerization of 2EPy within the galleries of MMT. The polymer thus formed is mostly bound to the surface of MMT at either the Brønsted or Lewis acid sites. Infrared analysis suggests the existence of positive charge on the nitrogen atom of the polymer inside the lamellar gallery. Bulk synthesized P2EPy—bulk in both protonated and deprotonated form—was also intercalated and studied by solid-state NMR. The variation in charge distribution of P2EPy intercalated under different conditions is also discussed.

Introduction

Layered aluminosilicates such as montmorillonites (MMTs) are well-suited for the synthesis of polymer nanocomposites. The exfoliated lamellae of MMT may act as a nanoscale host for polymer chains and may influence the structure and orientation of the intercalated macromolecules. Moreover, the lamellar aluminosilicates have been reported to be host for polymerization of acrylic monomers.^{1–8} The aggregates of MMT exfoliates partially or totally depending on the nature of monomer, medium, and the method of polymer–clay complex formation.^{5,9–11} These polymer/aluminosilicate nanocomposites frequently exhibit improved mechanical strength, improved thermal stability, interesting barrier properties, and chemical resistance.^{12–15}

Recently, we reported on a novel nanocomposite derived from intercalation and in-situ polymerization of an acetylenic monomer inserted into the galleries of MMT.^{11,16} The nanocomposite was synthesized by mixing the untreated MMT with a benzene solution of a pyridine-substituted acetylenic monomer, such as 2-ethynylpyridine (2EPy), the latter polymerizing spontaneously when adsorbed on the surface of the clay. Such an in-situ intercalative polymerization within montmorillonite appears to bear similarities with polymerizations reported earlier by Blumstein and co-workers concerning spontaneous polymerization of ethynyl derivatives endowed with a quaternizable atom (such as N, P, etc.) located alpha to the triple bond in contact with Brønsted or Lewis acid sites.¹⁷

The intercalation of the 2-ethynylpyridine was confirmed by the X-ray diffraction on samples of MMT with increasing adsorption yields of this monomer.¹¹ The

intercalated samples were subjected to solvent extraction with DMF (dimethylformamide) and a subsequent treatment with hydrofluoric acid to dissolve the silica–alumina matrix.¹⁶ However, such a drastic treatment of the clay organic complex may in some cases alter the structure of the polymer and destroy information about the clay–polymer interactions within the insertion complex.

Earlier studies on the extracted polymer by nondestructive methods—Fourier transform infrared (FT-IR) and ultraviolet visible (UV/vis) absorption spectroscopy—provided some useful information concerning the inserted polymer, such as for example the increase in conjugation with adsorption yield (red shift of the absorption maximum at 440 and 500 nm) or a clear evidence for the absence of the triple bond (disappearance of $\equiv\text{C}-\text{H}$ and $-\text{C}\equiv\text{C}-$ stretching bands at 3290 and 2110 cm^{-1} , respectively) after polymerization.^{11,16} These nondestructive methods, however, were qualitative and complicated by the low polymer content of the polymer–MMT nanocomposite,¹⁸ and destructive methods were necessary to study the structure and interactions of inserted polymers with their host lattice.^{1,11} Other traditional techniques used for the characterization of nanocomposites include XRD (measurement of basal d -spacing of clay minerals in nanocomposites) and transmission electron microscopy (TEM).^{9,19} However, most of the analytical and spectroscopic techniques are not suitable to study, without sample alteration, the structure, orientation, and local dynamics of the polymer chains inside the lamellar galleries. The development of tools for nondestructive methods of analysis is therefore an important task of research in the field of mineral–organic nanocomposites.

In recent years, solid-state nuclear magnetic resonance (NMR) spectroscopy specifically high-power proton-decoupled ^{13}C CP/MAS NMR has been established as

[†] Center for Advanced Materials.

[‡] Department of Chemistry.

* To whom all correspondence should be addressed.

one of the powerful tools for the investigation of structure, conformation, and dynamics of polymers and composites.^{20–22} The advantages of solid-state NMR are its ability to probe both the surface and the bulk of the polymer nondestructively. Application of solid-state NMR to study adsorbed substrates dates back to 1980, when Resing et al.²³ used ¹³C NMR to study the orientation of benzene rings within the interlayer space of the montmorillonite. Since then, this technique has been explored to study polymer–clay nanocomposites—the dynamics of adsorbed molecules on the mineral surface and their orientation inside the galleries.²⁴ Wang et al.²⁵ used variable temperature solid-state ¹³C NMR to report on conformational mobility and heterogeneity of surfactant molecules within the montmorillonite intercalation complex with emphasis on interfacial binding and chain conformation and dynamics.^{26–28} The broadening of the inner methylene resonances in the adsorbed surfactants compared to the bulk crystalline state was used to probe into the increase in chain mobility and conformational disorder.²⁸ In another study of PEO/montmorillonite nanocomposites,²⁹ ¹³C CP/MAS NMR was used to study the chain dynamics of intercalated PEO. Zax et al. studied intercalated PEO nanocomposites to determine the relative mobility of the bulk and interphase polymer^{30–32} and showed that the narrowing of the line width can be used to differentiate between the time scales of cation dynamics and the dynamics associated with segmental motion of the polymer. Multinuclear solid-state NMR was also used in a pioneering study of interaction of nylon-6 chains with the lamellae of aluminosilicate by Mathias et al.^{33–35}

VanderHart et al.^{36,37} recently studied the clay dispersion and stability of an organic modifier in different processing conditions of nylon-6/clay nanocomposites. Their results showed that the inherent paramagnetism of montmorillonite (mostly due to the presence of Fe³⁺ sites) could be used to establish the relative population of α - and γ -phases of the nylon-6 polymer in nanocomposites and used T_1^H values to measure the relative dispersion of proton relaxation times of the inserted chains.

Most of the NMR studies mentioned above are based on nanocomposites intercalated with polymers prepared outside the galleries of the clay or prepared by the use of an external initiator. In this paper, solid-state NMR is used to study the in-situ polymer obtained on the lamellar surface of MMT without pretreatment of the surface by an organic modifier or/and initiator. The goal in the present study is to focus on the structure of the formed polymer in the nanocomposite and its interactions with the clay surface, shedding some light on the initiation of the in-situ intercalative polymerization of 2EPy. Solid-state NMR, FT-IR, and XRD data suggest that under the above conditions a conjugated and charged polyacetylene located within the lamellae of MMT is formed. Polyacetylene prepared by bulk polymerization (P2EPy-bulk) outside of the lamellar clay is also intercalated into the galleries and forms an insertion compound, which is then compared with the in-situ prepared polymer using solid-state NMR techniques.

Experimental Section

Materials. Ca²⁺–montmorillonite (MMT) was purchased from Clay Minerals Repository with cation exchange capacity of 1.20 mequiv/g. 2-Ethynylpyridine (2EPy) was purchased from Farchan Laboratory. This sample was dried at 110 °C

for 24 h and then used without any further treatment. The concentration of sodium and calcium was determined by plasma atomic emission spectroscopy. The concentration of Ca²⁺ was 0.39 mmol/g, and the concentration of Na⁺ was essentially below the detection limit (for details, see ref 16). Clay Minerals Repository provided the following chemical composition: SiO₂ (60.4%), Al₂O₃ (17.6%), TiO₂ (0.24%), Fe₂O₃ (1.42%), FeO (0.08%), MnO (0.099%), MgO (6.46%), CaO (2.82%), Na₂O (0.063%), K₂O (0.19%), F (0.287%), P₂O₅ (0.020%). All other solvents and chemicals were analytical grade and used as received.

Synthesis of Poly(2-ethynylpyridinium hydrochloride) (P2EPy). 2EPy (2.06 g, 0.02 mol) was placed in a 250 mL flask and immersed in an ice bath. Concentrated HCl (2.0 g, 0.02 mol) was added dropwise. (*Caution should be exercised since this is a very exothermic reaction.*) After addition of approximately half of total hydrochloric acid (HCl) (1.2 mL), the reaction proceeded rapidly in 5 min, turning dark with rapid increase in viscosity of the reaction mixture. The polymer that was separated is a black mass. The reaction mixture was repeatedly washed with diethyl ether and dried in a vacuum at 40 °C. The dry polymer was obtained as a lustrous black powder (2.0 g) readily soluble in water and dimethyl sulfoxide (DMSO) and insoluble in chloroform.^{17f}

In-Situ Polymerization of Poly(2-ethynylpyridine)/MMT Nanocomposites. 0.395 g of 2EPy was added to a suspension of 1.0 g of dried MMT in 25 mL of benzene, and then the mixture was stirred at 65 ± 3 °C for 24 h.¹⁶ The dark brown precipitate was separated from suspension by centrifugation and washed several times with benzene to exclude the interstitial monomer trapped between the aggregates of clay particles. It was dried at 110 °C for 24 h. The adsorption yield of the monomer per unit weight of dried MMT, τ , was obtained by measuring the concentration of unreacted 2EPy in the benzene solution by UV/vis absorption spectroscopy.

Extraction of Polymer P2EPy from P2EPy/MMT Nanocomposites. 4.0 g of P2EPy/MMT complex was dispersed into 50 mL of dimethylformamide (DMF) and stirred at 85 °C for 1 h to extract the intercalated polymer from the complex. The dark red supernatant was separated from solid complex by centrifugation. The solid part was redispersed in 30 mL of fresh DMF, and the process was repeated. Finally, the DMF was removed from the combined solution by vacuum distillation at 45 °C (6 h), which yielded a dark brown solid mass. The solid was dissolved in methanol (~20 mL), and the solution was poured into 400 mL of cold ether to precipitate the solid polymer. The resulting dark brown solid was obtained by centrifugation and drying (0.056 g).

Deprotonation of Poly(2-ethynylpyridinium hydrochloride) (P2EPy). 0.5 g of the polymer was dissolved in 25 mL of deionized water and stirred. 50 mL of 1 M NaOH was slowly added and stirred continuously for 12 h. The deprotonated polymer was precipitated out as a dark solid and extracted with chloroform. The combined organic layers were dried with MgSO₄. Finally, the solvent was evaporated to yield a lustrous black solid (0.1 g), which was dried overnight in a vacuum.

Intercalation of Poly(2-ethynylpyridinium hydrochloride) and Its Deprotonated Form into MMT. 0.5 g of sample was dissolved in 25 mL of deionized water, and 1.0 g of MMT was added to it. The mixture was heated to 65 °C and stirred for 24 h. The black solid product (intercalated complex) was separated by centrifugation, washed with deionized water, and dried.

Characterization. The in-situ polymerized 2EPy in the interlamellar spacing of MMT was studied by X-ray powder diffraction and FT-IR.¹¹

NMR Spectroscopy. Solid-state ¹³C NMR experiments were carried out on a Bruker DMX 7.05 T widebore magnet system equipped with a 4 mm triple resonance broadband probe head. Zirconium oxide (ZrO₂) 4 mm (o.d.) rotors were used with Kel-F caps for all the measurements. The NMR measurements were carried out at room temperature. Cross-polarization with magic angle spinning (CP/MAS) and dipolar decoupling (DD) techniques were used to study these materi-

Table 1. Adsorption Yield (τ) and d -Spacing of Various Complexes Derived from in-Situ Polymerized 2-Ethynylpyridine within the Galleries of MMT

nanocomposite sample	adsorption yield (τ) ^a (%)	total area of aromatic resonance ^b	d -spacing ^c (nm)
NnC 1	8.0	1.00	1.49
NnC 2	15.3	1.35	1.58
NnC 3	21.3	1.50	1.64
P2EPy/MMT (bulk protonated)			1.89
P2EPy/MMT (bulk deprotonated)			1.48

^a The adsorption yield of polymer per unit weight of dehydrated Ca²⁺-montmorillonite. ^b The relative area determined from solid-state ¹³C CP/MAS NMR data. ^c The error range of the d -spacing is ± 0.05 nm (d -spacing of dehydrated Ca²⁺-montmorillonite is 0.96 nm).

als. A one-time magic angle adjustment was accomplished by maximizing the spinning sideband intensities of ⁷⁹Br NMR signal of KBr sample. All spectra were recorded using a rotor spinning speed of 10 kHz. The typical parameters for ¹³C CP/MAS NMR experiments were as follows: spin-lock field of 70 kHz, a 35 ms acquisition time, a 3 s recycle time, contact time of 1–2 ms, and sweep width of 31 kHz. The total number of free induction decays (FIDs) co-added per spectrum ranged from $\sim 10\,000$ for bulk polymer samples to 160 000 for the intercalated polymer-clay complex. All the FIDs were processed by exponential apodization function with a line broadening of 20–50 Hz. Variable contact time experiments were carried out to resolve the overlapping resonances and to determine the cross-polarization time constant (T_{CH}). All the ¹³C CP/MAS NMR spectra were externally referenced to glycine by assigning the carbonyl signal at 176.03 ppm with respect to tetramethylsilane (TMS).

Results and Discussion

In-Situ Polymerized P2EPy/MMT Nanocomposites. The in-situ intercalative polymerization of 2EPy–MMT complexes with increasing adsorption yields (τ) (Table 1) yields an increase in the d -spacing (d) and suggests intercalation of 2Epy. It ranged from $d = 1.49$ nm, corresponding to an adsorption yield of $\tau = 8.0\%$, to $d = 1.64$ nm with an adsorption yield of 21.3%.

A set of solid-state ¹³C CP/MAS NMR spectra of an in-situ polymerized 2EPy–MMT complex are shown in Figure 1 along with their chemical shift values for three different adsorption yields. An expanded solution-state ¹³C NMR spectrum (60–170 ppm) of the monomer (2EPy) is also shown as an insert in Figure 1. Comparing the spectra of both monomer (2EPy) and polymer (P2EPy), it is clear that the peaks due to the acetylenic carbons (82.9 and 77.7 ppm) are absent in the solid-state ¹³C NMR spectra of the polymer nanocomposites, indicating an almost complete and spontaneous (absence of an external initiator) polymerization of the monomer. As there are no carbons present in the MMT lattice, the signals observed in the ¹³C CP/MAS NMR spectra in Figure 1a–c are characteristics of the inserted polymer. The absence of triple bond and an increase in the d -spacing (XRD data) suggests an in-situ spontaneous intercalative polymerization of 2Epy. The resonances due to the ethylenic carbons of the P2Epy are not observed clearly due to their overlap with the resonances of pyridine rings. The solid-state ¹³C NMR spectrum appears as a broad distribution of resonances between 75 and 200 ppm. In all spectra, a strong peak appears at 126.0 ppm (labeled as peak A in Figure 1) along with a relatively weaker peak at 148 ppm (peak

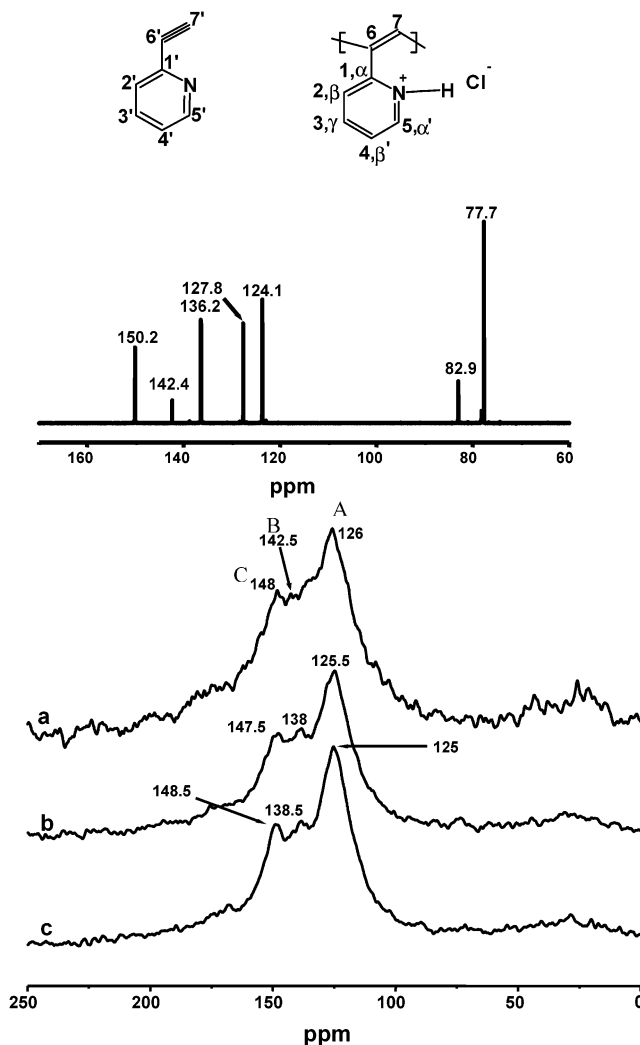
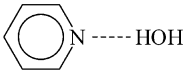
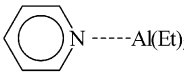
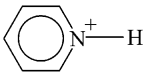


Figure 1. Solid-state ¹³C CP/MAS NMR spectra for in-situ polymerized 2-ethynylpyridine within the galleries of MMT: (a) NnC 1, (b) NnC 2, and (c) NnC 3. The inset shows the solution-state ¹³C NMR spectrum for 2-ethynylpyridine monomer.

C). Another partially resolved resonance at ~ 142.5 ppm (peak B) is also identified as a shoulder to the 148 ppm resonance in these spectra. Since cross-polarization is a measure of the efficiency of magnetization transfer from ¹H to ¹³C, the relative peak intensities for individual carbon species in the CP spectra reflect both the magnitude of dipolar coupling and the relative motions of C–H vectors. The fact that there is a sufficient polarization transfer allowing a reasonable signal-to-noise ratio even with such a low adsorption yield as 8% (Figure 1a) suggests the presence of highly anisotropic motions of the polymer chains inside the interlamellar space of the insertion complex.

With increasing adsorption yield, the signal-to-noise ratio increases along with the resolution (Figure 1b,c). All the ¹³C CP/MAS NMR spectra were recorded under the same experimental conditions. The number of scans accumulated for each spectrum was also kept constant in order to facilitate the quantification of solid-state ¹³C NMR data. The relative increase of total carbon signal intensity in the solid-state ¹³C NMR spectrum as a function of the adsorption yield appears linear (Table 1). With increase in the adsorption yield a new, resolved ¹³C NMR resonance peak can be identified (Figure 1b,c) at ~ 138 ppm along with other resonances at ca. 125 and

Table 2. ^{13}C Chemical Shift Assignments for Pyridine/Silica–Alumina³⁸

Nature of Bonding	Nature of Sample	$\Delta(\alpha-\beta)$ (in ppm)	$\Delta(\alpha-\gamma)$ (in ppm)
--	Liquid Pyridine	26.3	14.3
Hydrogen Bonded		25.1	12.8
Lewis acid-base interaction		21.6	6.9
Brønsted acid interaction		15.1 ^a	-4.3 ^a

^a Data obtained on solid pyridinium sulfate.

148 ppm. The partially resolved shoulder at ~ 142.5 ppm that appeared at lower adsorption yield (Figure 1a) shifted upfield to ~ 138 ppm at higher adsorption yields (Figure 1b,c). Resonances A, B, and C move upfield with increasing adsorption yields up to 16%. A further increase in the adsorption yield resulted in downfield shifts for peaks B and C, where as the peak A at 125 ppm is shifted upfield. The carbon resonances of the in-situ polymerized P2EPy/MMT nanocomposite samples are assigned by comparing the ^{13}C CP/MAS and CP/MAS combined with dipolar-dephasing NMR spectral data with previously published data for the chemical shift difference (Δ) on relevant model material systems (Table 2).³⁸ The ^{13}C NMR resonance assignments for liquid pyridine are as follows: C1 and C5 (α carbons) appear at 150.3 ppm, C2 and C4 (β carbons) appear at 124 ppm, and C3 (γ carbon) appears at 136 ppm. This gives the chemical shift difference (Δ) between $\Delta(\alpha-\beta)$ and $\Delta(\alpha-\gamma)$ carbons to be 26.3 and 14.3, respectively. The chemical shift difference (Δ) presented in Table 2 is dependent on the nature of bonding environments such as hydrogen bonding with dissociated water molecules, Lewis acid–base interaction with the exposed aluminum ions at the crystallite edges, and protonation, i.e., formation of a Brønsted complex. As the electron density on the nitrogen atom decreases, both $\Delta(\alpha-\beta)$ and $\Delta(\alpha-\gamma)$ decrease and in the case of a protonated sample, i.e., solid pyridinium sample, the γ carbon appears more downfield compared to α carbons showing negative $\Delta(\alpha-\gamma)$. Thus, the ^{13}C NMR chemical shifts or chemical shift differences (Δ) are sensitive to its local environments.

The tentative assignments of the three peaks A, B, and C in the solid-state ^{13}C NMR spectra of in-situ polymerized P2EPy/MMT nanocomposite are as follows: the ~ 125 ppm peak (peak A) corresponds to the ethylenic $-\text{CH}$ (C7) as well as the C2 and C4 (β and β') carbons of the pyridine ring. The peak at ~ 138 ppm (peak B) is due to the C3 (γ) carbon of the pyridine ring. (This peak appears at 142.5 ppm in the low adsorption yield ($\tau = 8\%$) P2EPy/MMT nanocomposite.) The resonance due to the ethylenic C (C6) that attached to aromatic ring is expected to appear at ~ 135 – 145 ppm and is not resolved in the solid-state ^{13}C NMR spectra of nanocomposite due to overlapping of broad resonances of pyridine ring carbons (Figure 1). The most downfield peak at ~ 148 ppm (peak C) is due to C1 and C5 (α and α'), both being attached to the nitrogen. Table 3 sum-

Table 3. ^{13}C Chemical Shift Assignments of 2-Ethynylpyridine and Poly(2-ethynylpyridine) within the Galleries of MMT

type of carbon	mono-mer	polymer (bulk protonated)	polymer (bulk deprotonated)	polymer (nanocomposite)
C1	150.1	147.0	155.5	148.5
C2	127.8	126.5	121.5	125
C3	136.2	147	136.0	138.5
C4	124.1	126.5	121.5	125
C5	142.4	147.0	149.5	148.5
$-\text{CH}=\text{}$		118.0	<i>a</i>	<i>a</i>
$\text{CH}\equiv$	77.7			
$\text{>C}=\text{}$		<i>a</i>	139.0	<i>a</i>
$-\text{C}\equiv$	82.9			

^a Not resolved, chemical shift in ppm.

marizes the chemical shift assignments for the monomer and the in-situ polymerized P2EPy/MMT nanocomposite.

Comparing the ^{13}C CP/MAS NMR spectra of the three nanocomposites, one significant observation, apart from variation in chemical shifts, is the decrease in the line broadening at higher adsorption yields. The line broadening in NMR is predominantly due to either spin diffusion (homogeneous broadening) or chemical shift dispersion (inhomogeneous broadening). In the present study, one possible contribution to the line broadening could arise from interaction of the polymer with fixed paramagnetic centers of the montmorillonite lattice and results in an electron spin induced relaxation of ^{13}C nuclei,³⁷ causing homogeneous spectral broadening due to a very short $T_{1\rho}(\text{H})$ at room temperature. However, the decrease in the line width of solid-state ^{13}C NMR spectrum with increased adsorption yield might be due to the increase of the number of polymer chains, which are probably away from fixed paramagnetic centers.

Protonated P2EPy-Bulk Polymer. To compare the structural similarity and the motional behavior of the intercalated polymer chains with the bulk polymer, we also synthesized P2EPy (P2EPy-bulk) in a strongly acidic medium.

The ^{13}C CP/MAS NMR spectrum of the synthesized P2EPy-bulk is presented in Figure 2A(a). The P2EPy-bulk shows well-resolved signals at 126.5 and 147.0 ppm along with a shoulder at 118.0 ppm. The tentative assignments are presented in Table 3. In contrast to the observed spectral feature for the in-situ polymerized sample, in the P2EPy-bulk prepared sample, the resonance at 136.2 ppm for C3 (γ) carbon of pyridine ring is shifted downfield due to structural changes that can be explained by the quaternization of the N atom in the pyridine ring.¹⁷ The positive charge on the quaternized nitrogen atom in the P2EPy-bulk polymer produced a downfield shift of the β and β' carbons by 2.5 ppm and γ carbons by 11 ppm and an upfield shift of the α and α' carbons by 3.5 ppm compared to the case of pure liquid pyridine.³⁸ Thus, the resonance for the γ carbon overlapped with the resonance of α and α' carbons showing a broad peak at 147 ppm for the P2EPy-bulk prepared polymer. These observations differ with the spectral features of the in-situ polymerized sample for which the γ carbon resonance is resolved from the α and α' carbon resonances. Other ring protonated carbons appear at ca. 126.5 ppm. The upfield shoulder at 118.0 ppm can be assigned to the ethylenic $-\text{CH}=\text{}$ (C7) carbon of the main chain.

Deprotonated P2EPy-Bulk Polymer. The ^{13}C CP/MAS NMR spectrum of the deprotonated P2EPy-bulk

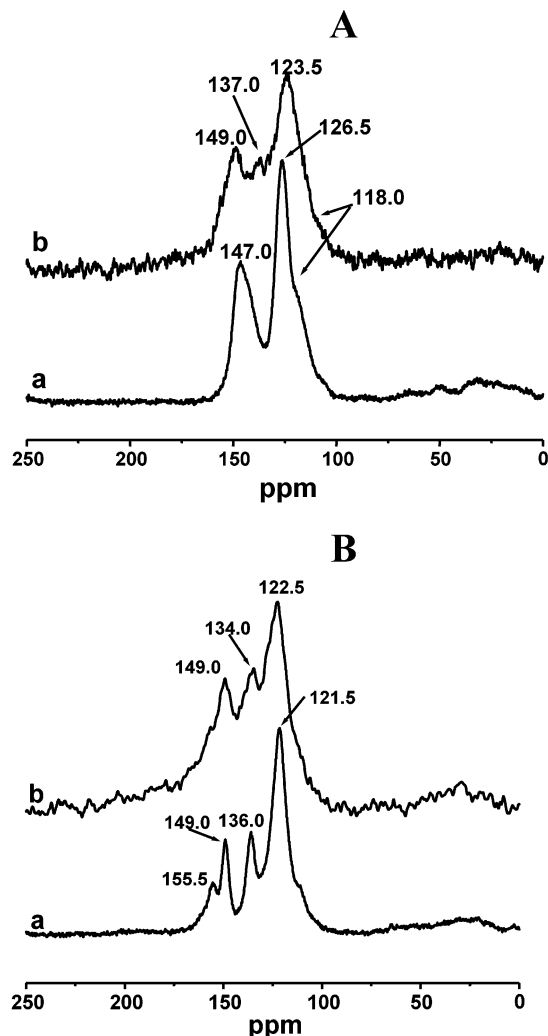


Figure 2. (A) Solid-state ^{13}C CP/MAS NMR spectra for (a) protonated P2EPy-bulk and (b) intercalated protonated P2EPy-bulk. (B) Solid-state ^{13}C CP/MAS NMR spectra of (a) deprotonated P2EPy-bulk and (b) intercalated deprotonated P2EPy-bulk.

is shown in Figure 2B(a), in which four distinct peaks are shown at 121.5, 136.0, 149.0, and 155.5 ppm. A shoulder peak is also clearly visible at 118.0 ppm. The major difference with the protonated bulk polymer (Figure 2A(a)) is the 5 ppm upfield shift of the 126.5 ppm peak due to β and β' carbons of the pyridine ring and the appearance of the downfield peak at 155.5 ppm. The removal of the positive charge on the nitrogen atom as a result of conversion to the deprotonated form showed in a downfield shift of the C1 (α) carbon from a broad resonance peak at 147 ppm. This allowed for the resolution of the peak at 149.0 ppm of the C5 (α') carbon of the pyridine ring. The C3 (γ) carbon shifted upfield and appeared at 136 ppm (similar to the chemical shift of the γ carbon of the liquid pyridine). After removal of the positive charge on the nitrogen atom by deprotonation, the chemical shifts of the ring carbons of the deprotonated P2EPy-bulk polymer resembled the liquid pyridine (Table 3).

High-resolution solution-state ^1H NMR as well as FT-IR spectra of protonated and deprotonated bulk polymers are presented in Figures 3 and 4. For the protonated polymer (Figure 3a), a broad hump is identified in the region of 4.5–6.5 ppm, which is absent in the case of deprotonated sample (Figure 3b), all other spectral

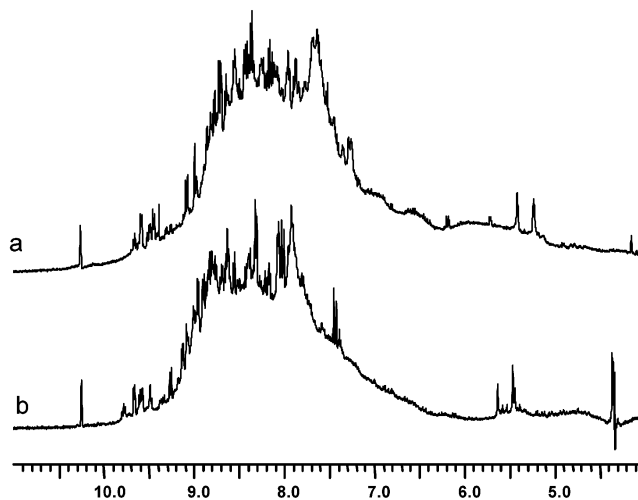


Figure 3. ^1H NMR spectra for (a) protonated P2EPy-bulk and (b) deprotonated P2EPy-bulk.

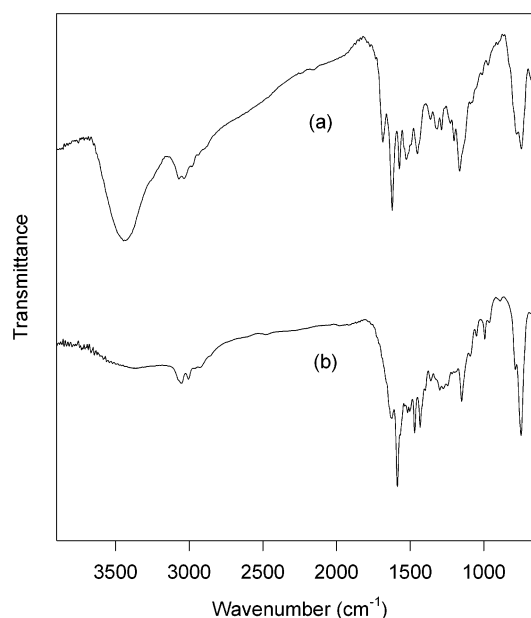


Figure 4. FT-IR spectra for (a) protonated P2EPy-bulk and (b) deprotonated P2EPy-bulk.

characteristics remaining the same. The hump can be assigned to the proton on the nitrogen atom bearing a positive charge that is neutralized during the deprotonation. This is also clear from the appearance of an intense vibration band at 3500 cm^{-1} in the FT-IR spectrum of the protonated bulk polymer for $-\text{NH}$ stretching (Figure 4a). The $-\text{NH}$ stretching ($\sim 3500 \text{ cm}^{-1}$) vibration band also decreased after the positive charge on the pyridine nitrogen atom was neutralized (Figure 4b). Earlier studies provided evidence for the presence of quaternized nitrogen atom in the P2EPy-bulk polymer. It was suggested that in the case of quaternization with a Brønsted acid 50% of the total nitrogens bear a positive charge. The protonated nitrogen atom is intramolecularly hydrogen bonded with the neighboring pyridine ring nonprotonated nitrogen.^{17f} Present investigation of the protonated and deprotonated P2EPy-bulk polymer suggests that the ring nitrogen in the as synthesized polymer remain protonated during the polymerization.

The presence of γ carbon resonance at ca. 138 ppm in the in-situ polymerized P2EPy/MMT nanocomposite

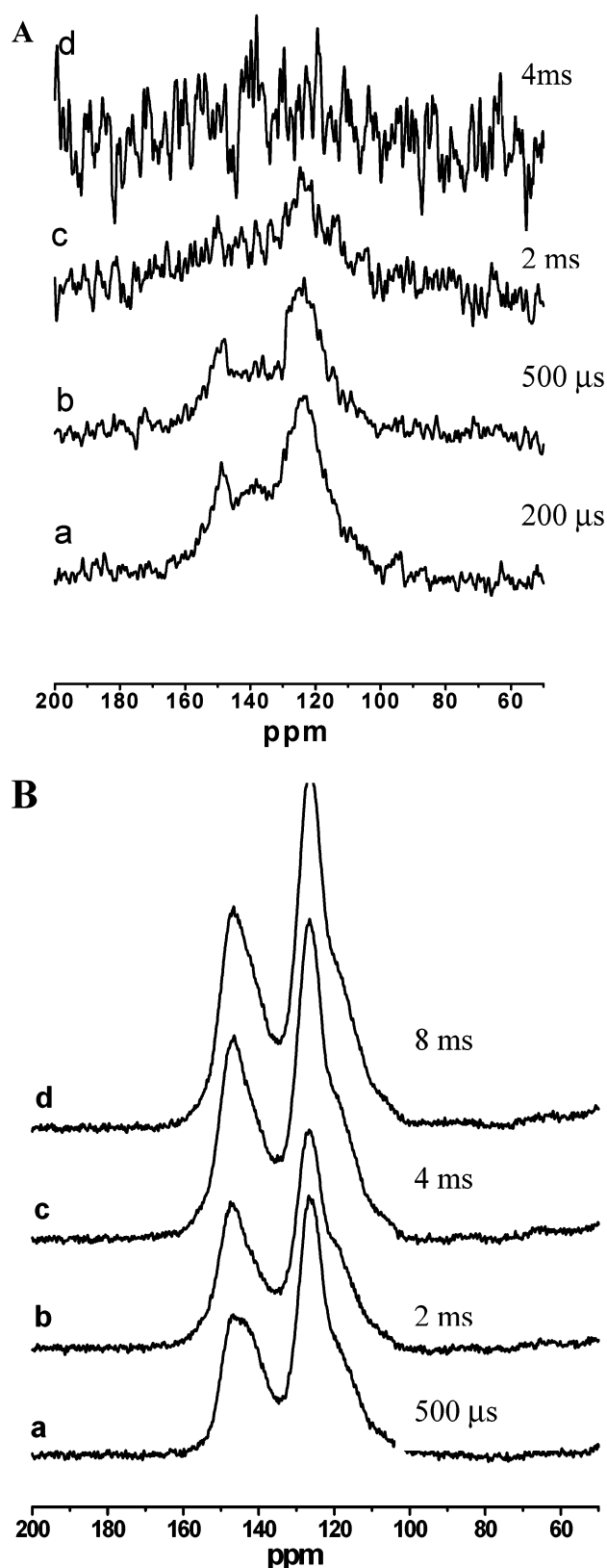


Figure 5. Variable contact time array spectra for (A) in-situ polymerized 2-ethynylpyridine within the galleries of MMT (NnC 3) and (B) P2EPy-bulk. The time shown for each spectrum is a contact time.

sample suggested that the nitrogen atom of the pyridine ring in the intercalated polymer is not fully protonated as it is in the P2EPy-bulk polymer sample. It is also likely that the interaction of the polymer with the surface of the montmorillonite resulted in the neutral-

ization of the charge density on the nitrogen. Figure 5 shows ^{13}C CP/MAS spectra recorded with varying values for the CP contact time on the bulk and the intercalated (complex 3) P2EPy (Figure 5) to check whether there is any effect of the motional averaging on the line shape. Since cross-polarization is efficient for the static ^{13}C – ^1H dipolar interactions, the less mobile carbon groups follow a faster cross-polarization route, resulting in a shorter T_{CH} . Thus, the T_{CH} can be used as a relative measure of the rigidity of polymer chain conformation. Variable contact time data on bulk P2EPy showed the highest intensity with 2 ms contact time and also mobility. In contrast, the polymer chains in the nanocomposite samples showed very short T_{CH} values. The highest intensity is at <1 ms contact time. This suggested that the polymer chains in the nanocomposite have a restricted mobility than in the bulk polymer.

The catalytic activity of the clay matrix is known to facilitate various organic transformations in heterogeneous catalysis.³⁹ The degree of isomorphous substitution influences the number and strength of surface acidity (Brønsted and Lewis acid sites) which in turn plays a major role in initiating the active sites for polymerization. Recent study on the intercalation and subsequent copolymerization of organic monomers inside galleries of lamellar clays shows that catalysis occurs at the clay mineral lattice edge where hydroxyl groups and exposed Al^{3+} ions at crystallite edges act as strong Brønsted and Lewis acid sites, respectively.⁴⁰

Despite extensive research performed on MMT–polymer systems, the nature of interactions of the polymer chains with the silica–alumina surface of the clay is not entirely clear. To explore the molecular dynamics of such systems, two nanocomposite samples were prepared by intercalation of the protonated and deprotonated P2EPy-bulk polymers into the galleries of MMT. As is shown in Table 1, intercalation takes place in both cases. The d -spacing is larger in the intercalated and protonated P2EPy-bulk polymer (1.89 nm) than deprotonated polymer (1.48 nm). ^{13}C CP/MAS NMR experiments on the intercalated P2EPy-bulk (protonated and deprotonated) polymers were compared with spectra of in-situ polymerized samples. These spectra are shown in parts A(b) and B(b) of Figure 2. After intercalation of the protonated polymer, the peaks broadened in comparison to bulk polymer, and the ^{13}C NMR spectral features are similar to the pattern of the in-situ polymerized nanocomposite sample. The NMR lines were broadened considerably after intercalation, probably due to the fast spin-induced relaxation of magnetization by interaction with the fixed paramagnetic centers within the lattice of the aluminosilicate. The peak at 126.5 ppm due to β and β' carbons shifted upfield to 123.5 ppm after intercalation while the downfield peak at 147 ppm due to α and α' carbons of the pyridine ring in the P2EPy-bulk shifted downfield to 149 ppm. Another peak appeared at 137 ppm after intercalation and may be due to the C3 (γ) carbons of the pyridine ring. The variation in chemical shifts is related to charge density on the nitrogen atom and suggests stronger association between the positive centers on the polymer and the negative charge on the lamellar surface of MMT.

The deprotonated P2EPy-bulk polymer shows similar spectral changes (Figure 2B(b)) upon intercalation as observed for the protonated bulk polymer (Figure 2A). However, the chemical shifts are different compared to

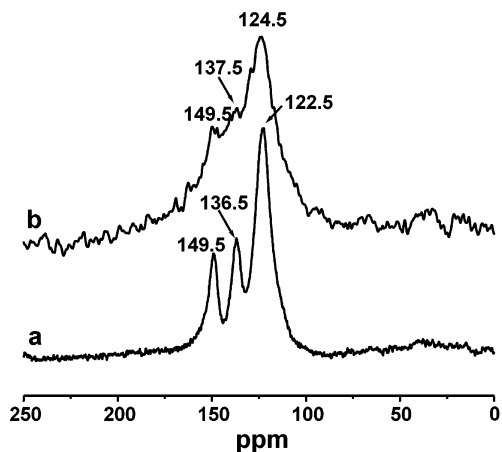


Figure 6. Solid-state ^{13}C CP/MAS NMR spectra for (a) extracted P2EPy from in-situ polymerized 2-ethynylpyridine within the galleries of MMT(NnC 2) and (b) residual NnC 2 after extraction.

the intercalated and protonated P2EPy-bulk sample. The protonated bulk intercalated P2EPy shows a much larger *d*-spacing (1.89 nm) than the deprotonated sample (1.48 nm). This suggests that the inserted polymer chains as well as their local environments are vastly different in both cases—the protonated polymer forming a tighter complex with a higher adsorption yield.

Extracted P2EPy from in-Situ Polymerized P2EPy/MMT Nanocomposite. The solid-state ^{13}C CP/MAS NMR spectrum of the extracted P2EPy was obtained after partial extraction of the polymer from the in-situ polymerized P2EPy/MMT nanocomposite sample (ca. 20% of the total polymer in the complex) is shown in Figure 6a. Figure 6b shows the ^{13}C CP/MAS NMR spectrum of the residual in-situ polymerized P2EPy/MMT nanocomposite after partial extraction of the polymer. The solid-state ^{13}C NMR spectral features of the extracted P2EPy polymer sample were similar to the one obtained from deprotonation of the bulk polymer except that resonances due to C1 and C5 are not resolved. This indicates that the charges on the nitrogens were neutralized in the extracted polymer. If the nitrogen were fully neutralized, the chemical shift of ^{13}C resonance would be similar to that of deprotonated bulk P2EPy (Figure 2B(a)). However, in the extracted P2EPy, the strong resonance was observed at 122.5 ppm, which is 1 ppm downfield compared to deprotonated bulk P2EPy. Also, the resonances for C1 and C5 (α and α' carbons) were not resolved in the extracted P2EPy. The presence of a small vibration band for $-\text{NH}$ stretching at ca. 3500 cm^{-1} supports the NMR data,¹¹ suggesting the presence of residual charges on the nitrogen atom. The spectral pattern of the residual nanocomposite (after extraction) resembled that of the parent nanocomposite spectrum (Figure 1b). There was only a slight variation in chemical shift values. It is expected that during the extraction all the loosely bound and interstitial polymers were preferentially removed from the polymer inserted into MMT.

The values for the ^{13}C NMR chemical shift difference $\Delta(\alpha-\beta)$ and $\Delta(\alpha-\gamma)$ for the in-situ polymerized P2EPy/MMT, the extracted polymer from in-situ polymerized P2EPy/MMT, the protonated, the deprotonated form of P2EPy-bulk, and the intercalated P2EPy-bulk samples are summarized in Table 4. For the protonated P2EPy-bulk polymer, the $\Delta(\alpha-\beta)$ value is 20.5 ppm while it is 27.5 ppm for the deprotonated P2EPy-bulk polymer. The

Table 4. ^{13}C Chemical Shift Difference (Δ) in Various P2EPy Polymer Samples

sample	$\alpha-\beta$	$\alpha-\gamma$	reference
NnC 1	22.0	5.5	Figure 1a
NnC 2	22.5	9.5	Figure 1b
NnC 3	23.5	10.5	Figure 1c
extd P2EPy	27.0	13.0	Figure 6a
P2EPy-bulk (protonated)	20.5		Figure 2A(a)
P2EPy-bulk (deprotonated)	27.5	13.0	Figure 2B(a)
intercalated P2EPy-bulk (protonated)	25.5	12.0	Figure 2A(b)
intercalated P2EPy-bulk (deprotonated)	26.5	15.0	Figure 2B(b)

$\Delta(\alpha-\gamma)$ values of the protonated P2EPy-bulk polymer cannot be determined because of overlapping of both resonances in the solid-state ^{13}C NMR spectrum (Figure 2A(a)). However, deprotonated P2EPy-bulk polymer shows a difference of 13 ppm between the chemical shifts of α and γ carbons ($\Delta(\alpha-\gamma)$). The data in Table 4 suggest the presence of a correlation between NMR parameters (Δ values) and the adsorption yield for in-situ polymerized P2EPy/MMT nanocomposite samples. The $\Delta(\alpha-\beta)$ and $\Delta(\alpha-\gamma)$ values increase with the adsorption yield. At low adsorption yield (τ) of 8%, $\Delta(\alpha-\beta)$ and $\Delta(\alpha-\gamma)$ values are 22 and 5.5 ppm, respectively. Comparison of these values with the model material systems (Table 2) indicates that at lower adsorption yield most of the polymer interacted with Lewis acid/base centers on the MMT surface defects. However, the increase of adsorption yield (τ) to 21.3% resulted in the increase of $\Delta(\alpha-\beta)$ and $\Delta(\alpha-\gamma)$ values to 23.5 and 10 ppm, respectively. This shows that hydrogen bonding is an important feature of adsorption. This may be because at a low adsorption yield the molecules are tightly bound to the montmorillonite surface by Lewis acid–base interactions.^{40,41} At higher adsorption yields a certain fraction of the molecules are hydrogen bonded. This appears to be reflected in the chemical shift difference values. The present study also suggests that the polymer intercalated with MMT is only partially protonated. This protonation may be due to the presence of trace of water solvating exchangeable cations or/and the presence of defects exposing their OH groups on the surface. It also proves the ability of polymer chains (bearing segmental charge or segmental dipole) to intercalate rapidly into the lamellar lattice of Ca^{2+} –MMT.

Conclusions

The results of solid-state ^{13}C NMR and X-ray diffraction studies unequivocally prove the formation of polymer (P2EPy) within the lamellar gallery of MMT as result of in-situ polymerization. The solid-state NMR data show that at lower adsorption yield the polymers are more tightly bound to the montmorillonite surface, and as the adsorption yield increases, the fraction of the loosely bound polymer increases. The solid-state NMR chemical shifts together with FT-IR data can be used as an indicator of extent of protonation in the in-situ polymerized P2EPy/MMT nanocomposites. The NMR spectral features of intercalated P2EPy-bulk polymers appear to be similar to the in-situ polymerized sample, and the positive charge on the nitrogen of the protonated P2EPy-bulk appears to be partially neutralized by the interaction with the negative charge of the surface of the montmorillonite. The polymer extracted from the nanocomposite P2EPy/MMT complex is in the

uncharged state. It displays similar NMR spectral features to that of a synthesized bulk polymer in the deprotonated state. The solid-state NMR spectrum of the remaining residual nanocomposite (after the extraction process) shows the presence of polymer bound to the MMT surface. The features of this spectrum are similar to that of in-situ polymerized nanocomposite with a low polymer yield.

Acknowledgment. We are indebted to the National Science Foundation (NSF Grant DMR-9986644) for the research grant. We thank to Mr. M. J. Downey for providing X-ray powder diffraction data.

References and Notes

- (1) (a) Blumstein, A. *Bull. Soc. Chim.* **1961**, 899. (b) Blumstein, A. *J. Polym. Sci.* **1965**, A3, 2653. (c) Blumstein, A.; Parikh, K. K.; Malhotra, S. L.; Blumstein, R. *J. Polym. Sci.* **1971**, A2, 9, 168. (d) Blumstein, A.; Blumstein, R. *Polym. Lett.* **1967**, 5, 691. (e) Blumstein, A.; Blumstein, R.; Vanderspurt, T. H. *J. Colloid Interface Sci.* **1969**, 31, 236. (f) Malhotra, S. L.; Parikh, K. K.; Blumstein, A. *J. Colloid Interface Sci.* **1972**, 41, 318.
- (2) Kojima, Y.; Usuki, A.; Kawasumi, M.; Okada, A.; Kurauchi, T.; Kamigaito, O. *J. Polym. Sci., Part A: Polym. Chem.* **1993**, 31, 1755.
- (3) Alexandre, M.; Dubois, P. *Mater. Sci. Eng., R* **2000**, 28, 1.
- (4) Huang, X.; Lewis, S.; Brittain, W. J.; Vaia, R. A. *Macromolecules* **2000**, 33, 2000.
- (5) Wang, Z.; Pinnavaia, T. J. *Chem. Mater.* **1998**, 10, 3769.
- (6) Vaia, R. A.; Jandt, K. D.; Kramer, E. J.; Giannelis, E. P. *Macromolecules* **1995**, 28, 8080.
- (7) (a) Friedlander, H. Z.; Frink, C. R. *J. Polym. Sci.* **1964**, B2, 475. (b) Vaia, R. A.; Giannelis, E. P. *Macromolecules* **1997**, 30, 8000.
- (8) (a) Kim, D. W.; Blumstein, A.; Kumar, J.; Tripathy, S. K. *Chem. Mater.* **2001**, 13, 243. (b) Kim, D. W.; Blumstein, A.; Tripathy, S. K. *Chem. Mater.* **2001**, 13, 1916.
- (9) (a) Krishnamoorti, R.; Vaia, R. A.; Giannelis, E. P. *Chem. Mater.* **1996**, 8, 1728. (b) Lemmon, J. P.; Wu, J.; Oriakhi, C.; Lerner, M. M. *Electrochim. Acta* **1995**, 40, 2245. (c) Ishida, H.; Campbell, S.; Blackwell, J. *Chem. Mater.* **2000**, 12, 1260.
- (10) Okamoto, M.; Morita, S.; Taguchi, H.; Kim, Y. H.; Kotaka, T.; Tateyama, H. *Polymer* **2000**, 41, 3887.
- (11) (a) Blumstein, A. *J. Polym. Sci.* **1965**, A3, 2665. (b) Liu, H.; Kim, D. W.; Blumstein, A.; Kumar, J.; Tripathy, S. K. *Chem. Mater.* **2001**, 13, 2756. (c) Kim, D. W.; Blumstein, A.; Liu, H.; Yang, S.; Kumar, J.; Tripathy, S. K. *Polym. Prepr.* **2001**, 42 (2), 3.
- (12) Garces, J. M.; Moll, D. J.; Bicerano, J.; Fibiger, R. McLeod, D. J. *Adv. Mater.* **2000**, 12, 1835.
- (13) Giannelis, E. P. *Adv. Mater.* **1996**, 8, 29.
- (14) Gomez-Romero, P. *Adv. Mater.* **2001**, 13, 163.
- (15) Eckle, M.; Decher, G. *Nano Lett.* **2001**, 1, 45.
- (16) Kim, D. W.; Blumstein, A.; Liu, H.; Downey, M. J.; Kumar, J.; Tripathy, S. K. *J. Macromol. Sci., Pure Appl. Chem.* **2001**, A38, 1405.
- (17) (a) Subramanyam, S.; Blumstein, A. *Macromol. Chem. Rapid Commun.* **1991**, 12, 23. (b) Blumstein, A.; Subramanyam, S. US Patent 5 037 916, 1991. (c) Blumstein, A.; Subramanyam, S. US Patent 5 104 948, 1992. (d) Blumstein, A.; Subramanyam, S. *Macromolecules* **1991**, 24, 2668. (e) Blumstein, A.; Subramanyam, S.; Li, K.-P. *Macromolecules* **1992**, 25, 2065. (f) Blumstein, A.; Subramanyam, S. *Macromolecules* **1992**, 25, 4058.
- (18) TGA data show that only 17% of the total polymer within the galleries of montmorillonite has been extracted from the complex by solvent treatment.
- (19) Usuki, A.; Kawasumi, M.; Yoshitsugu, K.; Okada, A.; Kurauchi, T.; Kamigaito, O. *J. Mater. Res.* **1993**, 8, 1174.
- (20) Bovey, F. A.; Mirau, P. A. *NMR of Polymers*; Academic Press: New York, 1996.
- (21) Schmidt-Rohr, K.; Spiess, H. W. *Multidimensional Solid-State NMR and Polymers*; Academic Press: London, 1994.
- (22) Engelhardt, G.; Michel, D. *High-Resolution Solid-State NMR of Silicates and Zeolites*; John-Wiley and Sons: Chichester, 1987.
- (23) Resing, H. A.; Slotfeld-Ellingsen, D.; Garroway, A. N.; Weber, D. C.; Pinnavaia, T. J.; Unger, K. *Magnetic Resonance in Colloid and Interface Science*; Fraissard, J. P., Resing, H. A., Eds.; Reidel: Boston, 1980; p 239.
- (24) Wang, L.-Q.; Exarhos, G. J.; Liu, J. *Adv. Mater.* **1999**, 11, 1331.
- (25) Wang, L.-Q.; Liu, J.; Exarhos, G. J.; Flanagan, K. Y.; Bordia, R. *J. Phys. Chem. B* **2000**, 104, 2810.
- (26) Gao, W.; Dickinson, L.; Grozinger, C.; Morin, F. G.; Reven, L. *Langmuir* **1997**, 13, 115.
- (27) Wang, L.-Q.; Liu, J.; Exarhos, G. J.; Bunker, B. C. *Langmuir* **1996**, 12, 2663.
- (28) Pawsey, S.; Yach, K.; Halla, J.; Reven, L. *Langmuir* **2000**, 16, 3294.
- (29) Kwiatkowski, J.; Whittaker, A. K. *J. Polym. Sci., Part B: Polym. Phys.* **2001**, 39, 1678.
- (30) Wong, S.; Vaia, R. A.; Giannelis, E. P.; Zax, D. B. *Solid State Ionics* **1996**, 86-88, 547.
- (31) Wong, S.; Zax, D. B. *Electrochim. Acta* **1997**, 42, 3513.
- (32) Yang, D.-K.; Zax, D. B. *J. Chem. Phys.* **1999**, 110, 5325.
- (33) Mathias, L. J.; Davis, R. D.; Jarrett, W. L. *Macromolecules* **1999**, 32, 7958.
- (34) Davis, R. D.; Jarrett, W. L.; Mathias, L. J. *Polym. Prepr.* **2001**, 42 (1), 55.
- (35) Davis, R. D.; Jarrett, W. L.; Mathias, L. J. *ACS Symp. Ser.* **2002**, 804, 117.
- (36) VanderHart, D. L.; Asano, A.; Gilman, J. W. *Macromolecules* **2001**, 34, 3819.
- (37) VanderHart, D. L.; Asano, A.; Gilman, J. W. *Chem. Mater.* **2001**, 13, 3781, 3796.
- (38) Maciel, G. E.; Haw, J. F.; Hawkins, B. L.; Early, T. A.; McKay, D. R.; Petrakis, L. *J. Am. Chem. Soc.* **1983**, 105, 5529.
- (39) Boudart, M. In *Principles of Heterogeneous Catalysis in Handbook of Heterogeneous Catalysis*; Ertl, G., Knozinger, H., Weitkamp, J., Eds.; Wiley-VCH: New York, 1997.
- (40) Stackhouse, S.; Coveney, P.; Sandre, E. *J. Am. Chem. Soc.* **2001**, 123, 11764.
- (41) Ukrainczyk, L.; Smith, K. A. *Environ. Sci. Technol.* **1996**, 30, 3167.

MA0258197